III-V-on-silicon 2-µm-wavelength-range wavelength demultiplexers with heterogeneously integrated InP-based type-II photodetectors

Ruijun Wang,[1,2,*] **Muhammad Muneeb,**[1,2] **Stephan Sprengel,**[3] **Gerhard Boehm,**[3] **Aditya Malik,**[1,2] **Roel Baets,**[1,2] **Markus-Christian Amann,**[3] **and Gunther Roelkens**[1,2]

[1]*Photonics Research Group, Ghent University-imec, Sint-Pietersnieuwstraat 41, B-9000 Ghent, Belgium*
[2]*Center for Nano- and Biophotonics (NB-Photonics), Ghent University, Ghent, Belgium*
[3]*Walter Schottky Institut, Technische Universität München, Am Coulombwall 4, 85748 Garching, Germany*
[*]*Ruijun.Wang@intec.ugent.be*

Abstract: 2-µm-wavelength-range silicon-on-insulator (SOI) arrayed waveguide gratings (AWGs) with heterogeneously integrated InP-based type-II quantum well photodetectors are presented. Low insertion loss (2.5-3 dB) and low crosstalk (−30 to −25 dB) AWGs are realized. The InP-based type-II photodetectors are integrated with the AWGs using two different coupling approaches. Adiabatic-taper-based photodetectors show a responsivity of 1.6 A/W at 2.35 µm wavelength and dark current of 10 nA at −0.5 V, while photodetectors using grating-assisted coupling have a responsivity of 0.1 A/W and dark current of 5 nA at −0.5 V. The integration of the photodetector array does not degrade the insertion loss and crosstalk of the device. The photodetector epitaxial stack can also be used to realize the integration of a broadband light source, thereby enabling fully integrated spectroscopic systems.

References and links

1. J. G. Crowder, S. D. Smith, A. Vass, and J. Keddie, "Infrared methods for gas detection," in *Mid-Infrared Semiconductor Optoelectronics* (Springer, 2006).
2. M. N. Petrovich, F. Poletti, J. P. Wooler, A. M. Heidt, N. K. Baddela, Z. Li, D. R. Gray, R. Slavík, F. Parmigiani, N. V. Wheeler, J. R. Hayes, E. Numkam, L. Grűner-Nielsen, B. Pálsdóttir, R. Phelan, B. Kelly, J. O'Carroll, M. Becker, N. MacSuibhne, J. Zhao, F. C. Gunning, A. D. Ellis, P. Petropoulos, S. U. Alam, and D. J. Richardson, "Demonstration of amplified data transmission at 2 µm in a low-loss wide bandwidth hollow core photonic bandgap fiber," Opt. Express **21**(23), 28559–28569 (2013).
3. N. Ye, M. Gleeson, M. Sadiq, B. Roycroft, C. Robert, H. Yang, H. Zhang, P. Morrissey, N. M. Suibhne, K. Thomas, A. Gocalinska, E. Pelucchi, R. Phelan, B. Kelly, J. O'Carroll, F. Peters, F. G. Gunning, and B. Corbett, "InP-Based active and passive components for communication systems at 2 µm," J. Lightwave Technol. **33**(5), 971–975 (2015).
4. G. Roelkens, U. Dave, A. Gassenq, N. Hattasan, C. Hu, B. Kuyken, F. Leo, A. Malik, M. Muneeb, E. Ryckeboer, D. Sanchez, S. Uvin, R. Wang, Z. Hens, R. Baets, Y. Shimura, F. Gencarelli, B. Vincent, R. Loo, J. Van Campenhout, L. Cerutti, J. B. Rodriguez, E. Tournie, X. Chen, M. Nedeljkovic, G. Mashanovich, L. Shen, N. Healy, A. C. Peacock, X. Liu, R. Osgood, and W. Green, "Silicon-based photonic integration beyond the telecommunication wavelength range," IEEE J. Sel. Top. Quantum Electron. **20**(4), 394–404 (2014).
5. A. Subramanian, E. M. P. Ryckeboer, A. Dhakal, F. Peyskens, A. Malik, B. Kuyken, H. Zhao, S. Pathak, A. Ruocco, A. De Groote, P. C. Wuytens, D. Martens, F. Leo, W. Xie, U. D. Dave, M. Muneeb, P. V. Dorpe, J. V. Campenhout, W. Bogaerts, P. Bienstman, N. L. Thomas, D. V. Thourhout, Z. Hens, G. Roelkens, R. Baets, "Silicon and silicon nitride photonic circuits for spectroscopic sensing on-a-chip," Photonics Research **5**(3), 47–59 (2015).
6. M. Smit and C. Van Dam, "PHASAR-based WDM-devices: Principles, design and applications," IEEE J. Sel. Top. Quantum Electron. **2**(2), 236–250 (1996).
7. W. Bogaerts, S. K. Selvaraja, P. Dumon, J. Brouckaert, K. De Vos, D. Van Thourhout, and R. Baets, "Silicon-on-insulator spectral filters fabricated with CMOS technology," IEEE J. Sel. Top. Quantum Electron. **16**(1), 33–44 (2010).
8. M. Muneeb, X. Chen, P. Verheyen, G. Lepage, S. Pathak, E. Ryckeboer, A. Malik, B. Kuyken, M. Nedeljkovic, J. Van Campenhout, G. Z. Mashanovich, and G. Roelkens, "Demonstration of Silicon-on-insulator mid-infrared spectrometers operating at 3.8 µm," Opt. Express **21**(10), 11659–11669 (2013).

9. E. Ryckeboer, A. Gassenq, M. Muneeb, N. Hattasan, S. Pathak, L. Cerutti, J. B. Rodriguez, E. Tournié, W. Bogaerts, R. Baets, and G. Roelkens, "Silicon-on-insulator spectrometers with integrated GaInAsSb photodiodes for wide-band spectroscopy from 1510 to 2300 nm," Opt. Express **21**(5), 6101–6108 (2013).
10. H. Nishi, T. Tsuchizawa, R. Kou, H. Shinojima, T. Yamada, H. Kimura, Y. Ishikawa, K. Wada, and K. Yamada, "Monolithic integration of a silica AWG and Ge photodiodes on Si photonic platform for one-chip WDM receiver," Opt. Express **20**(8), 9312–9321 (2012).
11. R. Yu, R. Proietti, J. Kurumida, A. Karalar, B. Guan, and S. J. B. Yoo, "Rapid high-precision in situ wavelength calibration for tunable lasers using an athermal AWG and a PD array," IEEE Photonics Technol. Lett. **24**(1), 70–72 (2012).
12. R. Wang, S. Sprengel, M. Muneeb, G. Boehm, R. Baets, M. C. Amann, and G. Roelkens, "2 μm wavelength range InP-based type-II quantum well photodiodes heterogeneously integrated on silicon photonic integrated circuits," Opt. Express **23**(20), 26834–26841 (2015).
13. K. Okamoto, "Wavelength-Division-Multiplexing Devices in Thin SOI: Advances and Prospects," IEEE J. Sel. Top. Quantum Electron. **20**(4), 248–257 (2014).
14. S. Sprengel, A. Andrejew, K. Vizbaras, T. Gruendl, K. Geiger, G. Boehm, C. Grasse, and M.-C. Amann, "Type-II InP-based lasers emitting at 2.55 μm," Appl. Phys. Lett. **100**(4), 041109 (2012).
15. S. Sprengel, G. K. Veerabathran, F. Federer, A. Andrejew, and M.-C. Amann, "InP-Based Vertical-Cavity Surface-Emitting Lasers With Type-II Quantum Wells," IEEE J. Sel. Top. Quantum Electron. **21**(6), 1701309 (2015).
16. S. Keyvaninia, M. Muneeb, S. Stankovic, P. J. V. Veldhoven, D. V. Thourhout, and G. Roelkens, "Ultra-thin DVS-BCB adhesive bonding of III–V wafers, dies and multiple dies to a patterned silicon-on-insulator substrate," Opt. Mater. Express **3**(1), 35–46 (2013).
17. N. Hattasan, A. Gassenq, L. Cerutti, J. B. Rodriguez, E. Tournie, and G. Roelkens, "Heterogeneous integration of GaInAsSb p-i-n photodiodes on a silicon-on-insulator waveguide circuit," IEEE Photonics Technol. Lett. **23**(23), 1760–1762 (2011).
18. C. B. Li, R. W. Mao, Y. H. Zuo, L. Zhao, W. H. Shi, L. P. Luo, B. W. Cheng, J. Z. Yu, and Q. M. Wang, "1.55 μm Ge islands resonant-cavity-enhanced detector with high-reflectivity bottom mirror," Appl. Phys. Lett. **85**(14), 2697–2699 (2004).

1. Introduction

The 2 μm wavelength range is of interest for the spectroscopic detection of several important industrial gases [1]. Besides, recently improved transmission and amplification capabilities of hollow-core photonic-bandgap fibres promise a new telecommunication window at wavelengths around 2 μm [2]. Therefore, the development of integrated photonic systems for the 2 μm wavelength range has attracted much attention for these applications [3,4]. The integration of a wavelength demultiplexer and photodetector array operating in the 2 μm wavelength range is of key importance for both types of applications. As a widely used (de)multiplexer in wavelength division multiplexing (WDM) systems, arrayed waveguide gratings (AWGs) can also be applied for spectroscopic sensing [5]. High performance AWGs have been demonstrated in several low-index-contrast material systems, such as silica [6]. However, the footprint of these AWGs is usually very large. As a high-index-contrast material system, the silicon-on-insulator (SOI) platform can be used to fabricate waveguides with a tight bending radius, and consequently ultracompact AWGs [7]. Moreover, the silicon photonics waveguide platform can leverage the standard silicon electronics process technology, a large asset when envisaging high-volume manufacturing and the dense co-integration with electronics. In recent years, AWG demultiplexers based on the silicon photonics platform have been demonstrated in wavelength ranges beyond the classical telecommunication window [8,9]. E. Ryckeboer *et al*. reported a low resolution (4.8 nm) and high resolution (1.6 nm) AWG spectrometer based on strip SOI waveguides having a crosstalk of −12 dB and −16 dB and an insertion loss of 2.1 dB and 4 dB, respectively [9]. As crosstalk significantly influences spectroscopic sensing performance it should be as low as possible. In this paper, we demonstrate low insertion loss (2.5-3 dB) and low crosstalk (−30 to −25 dB) AWGs operating in the 2.3-2.4 μm wavelength range with different resolutions. All of these AWGs are fabricated based on a shallow-etched SOI waveguide platform.

The integration of a photodetector array on these wavelength demultiplexers is also addressed in this work. For telecommunication applications, the integration of an AWG demultiplexer with a photodetector array allows realizing a WDM receiver [10]. For spectroscopic applications, it is the first step towards a fully integrated spectroscopic sensing system [11]. The transfer of III-V material by adhesive bonding or molecular bonding is an

efficient and scalable method to integrate III-V photodetectors on SOI. For the 2 µm wavelength range, either GaSb-based type-I or InP type-II heterostructures can be used to realize high performance photodetectors. Compared with the GaSb-based material system, the heterogeneous integration processes for InP-based materials is much more mature resulting in higher device yield and better device performance. Recently, we demonstrated a heterogeneously integrated adiabatically-coupled InP-based type-II photodetector on SOI with a responsivity of 1.2 A/W at a wavelength of 2.32 µm [12]. In this paper, we present 2-µm-wavelength-range SOI AWGs co-integrated with an InP-based type-II quantum well photodetector array. Adiabatic coupling and grating-assisted coupling is compared, using the same III-V epitaxial layer stack. The adiabatically-coupled photodetectors have a responsivity of 1.6 A/W at wavelength of 2.35 µm and dark current of 10 nA at −0.5 V bias at room temperature. The grating-assisted photodetectors have better fabrication tolerance and show a responsivity of 0.1 A/W and dark current of 5 nA at −0.5 V bias. Both kinds of heterogeneously integrated photodetectors show good processing yield. The integration of the photodetector array does not degrade the insertion loss and crosstalk of the device. The photodetector epitaxial layer stack is also used to realize the integration of a broadband light source, thereby enabling fully integrated spectroscopic systems on silicon photonic chips.

2. Passive AWG wavelength demultiplexers

The SOI waveguides are fabricated on 200 mm SOI wafers in imec's CMOS pilot line. The SOI wafer consists of a 400 nm thick silicon device layer on a 2 µm buried oxide layer. The silicon waveguide patterns are defined by 193 nm deep UV lithography. Inductively-coupled plasma (ICP) dry etching is used to etch 180 nm deep silicon rib waveguides. Afterwards, a layer of SiO_2 is deposited on the SOI wafer and planarized by a chemical mechanical polishing (CMP) process. Figure 1 shows the microscope images of a fabricated low resolution and high resolution AWG. The AWGs consist of two free propagation regions (FPRs) and 32 arrayed waveguides (known as delay lines) with constant length increment located between the two FPRs. When the light enters the input aperture through a 3 µm wide waveguide as shown in Fig. 1(b), it diverges and couples into the waveguide array (2 µm wide waveguides with a pitch of 2.2 µm) at the end of the FPR. After passing through the waveguide array, different wavelengths will be refocused on a certain 3 µm wide output waveguide in the output aperture. The path length difference between the delay lines is 30.8 µm / 108.3 µm for the low resolution and high resolution device respectively. The footprint of the low resolution and high resolution AWG is 0.45 mm^2 and 1.1 mm^2, respectively. Detailed information about the principle of AWG design can be found in [6]. Four different AWGs designed for the 2.3-2.4 µm wavelength range are presented in this work. All of the AWGs are designed for TE polarized light. The detailed AWG design parameters are summarized in Table 1.
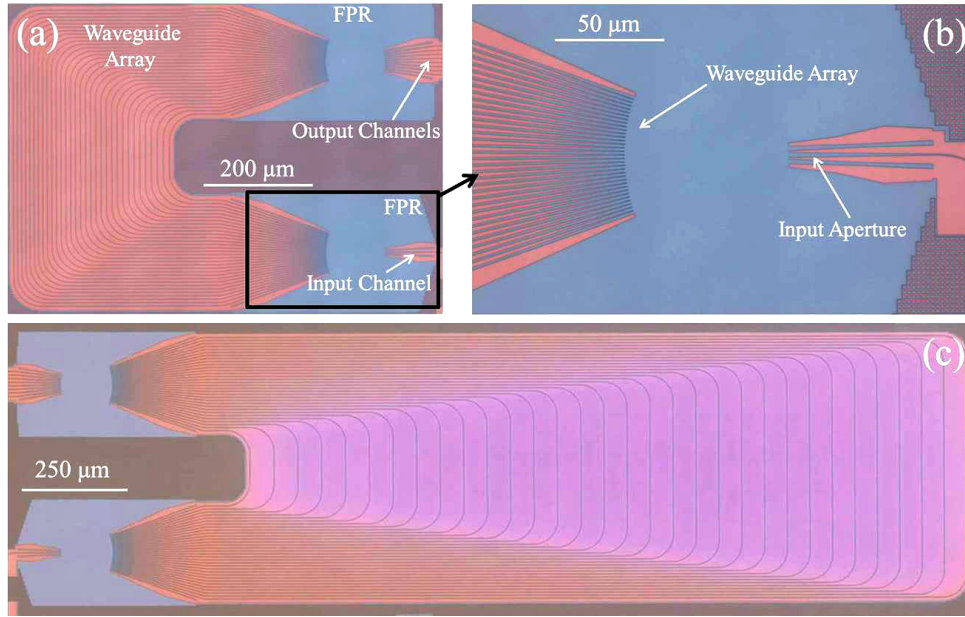
Fig. 1. Microscope image of (a) the low resolution AWG; (b) magnification of the input section of the low resolution AWG; (c) the high resolution AWG.

Table 1. Design and Layout Parameters Summary for AWGs

	AWG1	AWG2	AWG3	AWG4
Center wavelength (nm)	2375	2375	2375	2375
FSR (nm)	50	14.1	18.8	59.2
Channel spacing (nm)	5	1.41	3.76	4.23
No. of arrayed waveguides	32	32	20	48
FPR length (μm)	108	108	98.15	235.46
Single mode WG width (nm)	826	826	826	826
Expanded WG width (μm)	1.5	1.5	1.5	1.5
Taper length (μm)	90	90	90	90
Bend radius (μm)	50	50	50	50
Aperture width (μm)	3	3	3	3
Space between WGs (nm)	200	200	200	200
Device size: L × W (mm × mm)	0.78 × 0.57	1.98 × 0.57	1.06 × 0.57	0.94 × 0.68

The passive device performance is characterized by measuring the transmission spectrum of each channel. TE polarized light tuned with a step of 0.1nm from a tunable Cr^{2+}:ZnSe solid state laser is coupled to the input channel of the AWG through a 20 μm × 20 μm grating coupler with a grating period of 1 μm (50% duty cycle). An optical spectrum analyzer (OSA, Yokogawa AQ6375) is used to collect light from different output grating couplers. The insertion loss and crosstalk of the AWGs is acquired by normalizing the transmission spectra of the AWGs to a reference waveguide. Figure 2(a) and 2(b) show the spectral responses of all the 8 channels in the low resolution and high resolution AWG, which correspond to the devices shown in Fig. 1(a) and 1(c), respectively. From the measurement, it can be found that the insertion loss is around 2.5 dB and the crosstalk level is −30 dB for the low resolution AWG (AWG-1) as shown in Fig. 2(a). The high resolution AWG (AWG-2) has an insertion loss of about 2.8 dB and crosstalk level of −25 dB. The low resolution and high resolution AWG has a channel spacing of 5 nm and 1.4 nm, respectively. Figure 2(c) shows a 5 channel AWG (AWG-3) that has an insertion loss of about 2.5 dB and crosstalk level of −26 dB and Fig. 2(d) shows a 12 channel AWG (AWG-4) that has an insertion loss of about 3 dB and a crosstalk level of −28 dB. AWG-3 and AWG-4 have a channel spacing of 3.8 nm and 4 nm,

respectively. All four AWGs show a good channel uniformity. The performance of these 2-µm-wavelength-range AWGs is comparable with state-of-the-art SOI AWGs at classical telecommunication wavelengths [13].
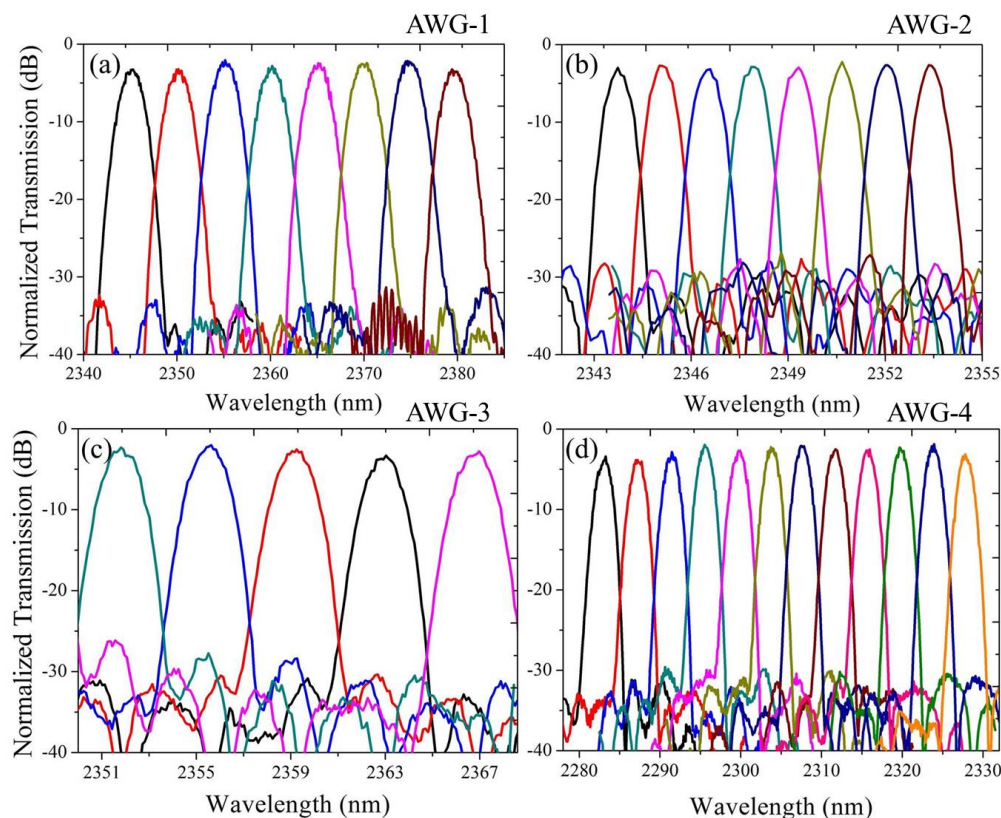

Fig. 2. The measured spectral responses of all the channels in four different AWGs.

3. InP-based type-II opto-electronic device integration onto silicon photonic ICs

For a fully integrated spectroscopic system, light sources, photodetectors and passive components should be integrated on the same chip. The epitaxial structure of the photodetectors used in this work can also be used to integrate 2-µm-wavelength-range light sources on the SOI waveguide platform. This way, all of the active components required for the spectroscopic sensing system can be realized using a single epitaxial layer stack and process flow. The III-V epitaxial layer stack, including "W"-shaped quantum well structures, is grown on an InP substrate with a molecular beam epitaxy (MBE) system. The detailed information about the epitaxial structure can be found in [12]. The active region of the photodetector is comprised of six periods of a "W"-shaped quantum well structure, each separated by 9 nm tensile strained GaAsSb layers. The inset of Fig. 3 depicts the band structure of one period of the active region. It consists of one 2.9 nm GaAsSb layer confining the holes, surrounded by two 2.6 nm InGaAs layers, confining the electrons. This active region design can be used for the realization of 2-µm-wavelength-range LEDs, lasers [14,15] or photodetectors. Figure 3 shows the electroluminescence (EL) spectrum from a heterogeneously integrated 8 µm × 450 µm InP-based type-II waveguide-coupled LED on SOI (100 mA bias). A broadband emission between 2.2 µm and 2.45 µm with peak position at 2.35 µm is coupled to the silicon waveguide. The light is coupled from the active region to the silicon waveguide by a 180 µm long linearly tapered III-V waveguide with a taper tip width of around 500 nm.
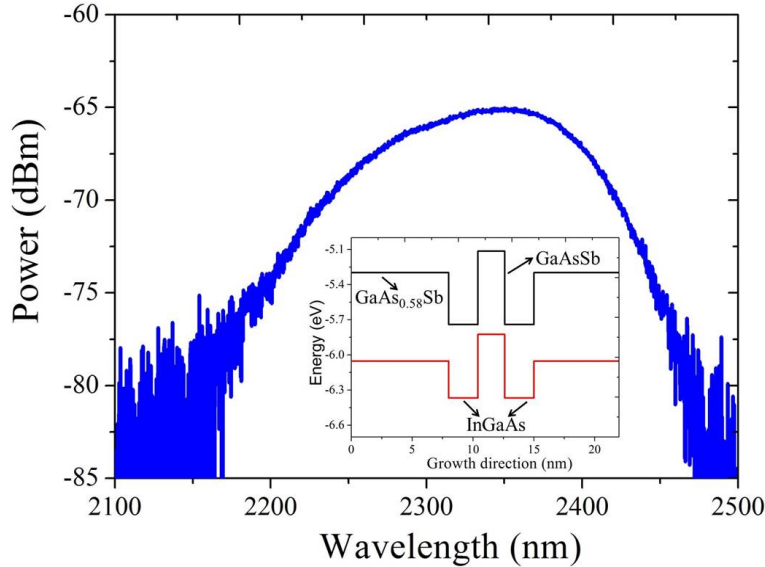
Fig. 3. EL spectrum from a heterogeneously integrated InP-based type-II LED (100 mA bias).
The inset picture shows the band structure of one "W"-shaped period of the active region.

Figure 4 schematically shows the cross-section of the heterogeneously integrated InP-based type-II devices (LEDs and photodetectors) on SOI. The integration process flow starts with transferring a III-V epitaxial layer stack to SOI by adhesive bonding using Benzocyclobutene (DVS-BCB). The specifics of the bonding process are described in [16]. After bonding, the InP substrate is removed using a HCl solution. Then the III-V mesa of the photodetector is processed on the III-V membrane. Firstly, a 200 nm SiN_x layer is patterned to serve as the hardmask for the p-InP mesa etching. The 100 nm p^+-InGaAs layer is etched by ICP (using $CH_4:H_2$ = 30:10 sccm) and the 1.5 μm p-InP cladding layer is etched by using a 1:1 $HCl:H_2O$ solution. The III-V mesa is oriented along [01-1] direction. This way the anisotropic HCl wet etching of InP creates an inverted trapezoidal mesa. This is a key technological process for adiabatically-coupled photodetectors because it can reduce the lithographic requirements for the narrow taper tip fabrication. For a 1 μm taper tip on the hard mask, the bottom width of p-InP cladding layer is reduced to 200 nm. So tapered III-V waveguides with a very narrow tip can be defined by using 320 nm UV contact lithography. Afterwards, a SiN_x layer is deposited and patterned on the sample to protect the InP taper in the following wet etching process and at the same time also passivating the thick p-InP mesa. Subsequent wet etching of the multiple quantum well structure is done using 1:1:20:70 $H_3PO_4:H_2O_2:CitricAcid:H_2O$. Then Ni/Ge/Au is deposited onto the exposed n-InP layer, 5 μm away from the edge of the III-V mesa. After metal lift-off, the n-InP layer is etched by a diluted HCl solution for device isolation. Then the structure is encapsulated with DVS-BCB for device passivation. After curing, the DVS-BCB is etched by reactive ion etching (RIE) (using $SF_6:O_2$ = 5:50 sccm) for the opening of the n-contacts and the p-contacts. Finally, Ti/Au is deposited as the n-contact and p-contact probe pad.
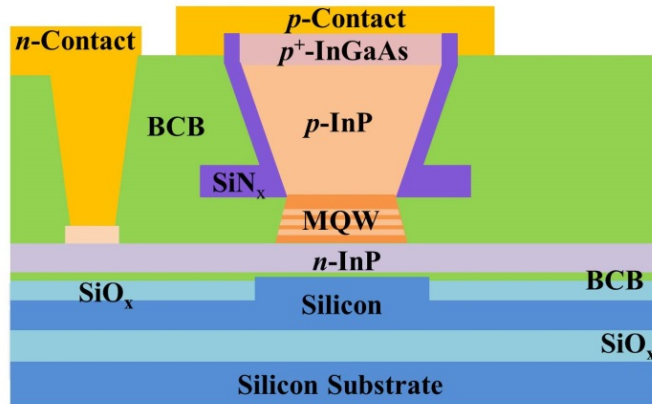
Fig. 4. Schematic of the cross-section of the photodetector/LED structure.

4. AWGs integrated with an adiabatically-coupled photodetector array

The top view of the adiabatically-coupled photodetector is schematically shown in Fig. 5(a), showing the photodetector mesa only for clarity. The III-V mesa of the heterogeneously integrated photodetector is a 150 µm long waveguide, tapered from 1 µm to 3.5 µm (the width of SiN_x hard mask pattern). The silicon waveguide below the III-V mesa is a 3 µm wide rib waveguide. Light can be efficiently coupled from the silicon waveguide to the active region by the narrow inverted trapezoidal taper tip (200 nm width at the bottom of the p-InP as discussed above). Figure 5(b) shows the scanning electron microscope (SEM) cross-section image of the photodetector. A 100 nm thick DVS-BCB layer is used as bonding agent for the heterogeneous integration.
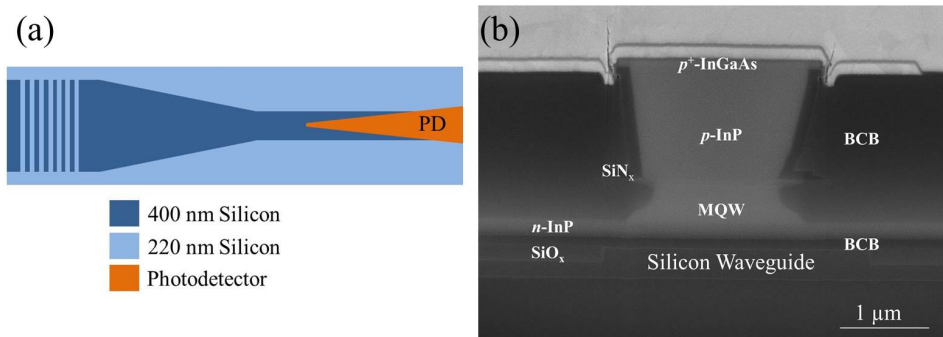

Fig. 5. (a) Schematic drawing of the top view of the adiabatically-coupled photodetectors on SOI waveguides; (b) SEM image of the cross-section of the device.

Figure 6(a) shows a typical current-voltage (I-V) curve of the adiabatically-coupled photodetectors without light input. The measured average dark current is around 10 nA at a bias voltage of -0.5 V. This is several orders of magnitude lower than previously demonstrated waveguide-coupled GaSb-based photodetectors (1.13 µA at −0.1 V) [17], which can be attributed to the use of better developed InP processes, the SiN_x passivation of the thick p-InP cladding layer and the timely passivation of the photodetector using DVS-BCB. The optical response of the photodetectors at 2.35 µm wavelength under different optical input powers in the silicon waveguide is shown in Fig. 6(b). The actual optical power coupled to the silicon waveguides is determined by measuring a reference SOI waveguide with the same grating coupler as on the real device structure. The waveguide-referred responsivity is around 1.6 A/W, which corresponds to a quantum efficiency of 85%. The linearity of the photodetector is analyzed in Fig. 6(c). At 0 V bias the photodetector linear operation is

obtained for optical input powers below 200 µW. For linear operation at higher optical input power, a reverse bias is required to extract all photogenerated carriers. Under a reverse bias voltage of 1 V, linear operation is obtained up to an optical input power of around 630 µW, which is the maximum power that can be obtained from our light source.
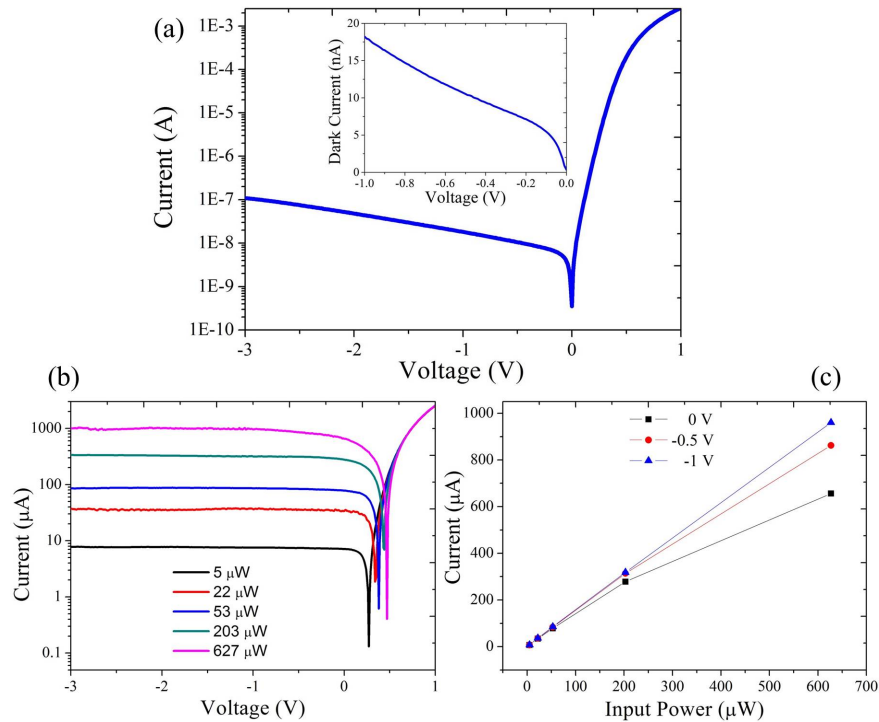

Fig. 6. (a) I-V curve of the adiabatically-coupled photodetectors without light input, the inset figure shows the dark current of the devices; (b) photoresponse of the devices under different input power levels; (c) Linearity analysis of the adiabatically-coupled III-V-on-silicon photodetectors.

Figure 7(a) shows a microscope image of the low resolution AWG (AWG-1, shown in Fig. 1(a)) integrated with adiabatically-coupled photodetectors. All of the eight channels are integrated with photodetectors, the pitch of which is 60 µm. A reference photodetector is fabricated for photodetector characterization and insertion loss measurement of the AWG spectrometers after III-V processing. In device measurements, TE-polarized light from the tunable laser source is coupled to a standard single mode fiber (SMF-28) and then split by a 1/99 splitter. The 1% port is connected to the OSA as a wavelength and power reference. The light in 99% path is coupled to the AWG spectrometer and read out through the heterogeneously integrated photodetectors. The photodetectors are probed individually and the photocurrent is acquired by a Keithley SourceMeter. Figure 7(b) and 7(c) display the photoreponse of two AWGs (AWG-1 and AWG-3) integrated with adiabtically-coupled photodetectors. The bias voltage is fixed at −0.5 V. By normalizing the responsivity with the reference photodetector, an insertion loss of 3 dB and a crosstalk level of −27 dB are obtained for AWG-1. With integrated photodetectors, the AWG-3 has an insertion loss of 3.5 dB and crosstalk level of −29 dB as shown in Fig. 7(c), illustrating the fact that the post-processing doesn't affect the spectrometer performance substantially. A red-shift in the recorded spectra after photodetector integration can be observed, which is due to the DVS-BCB cladding applied during the photodetector array processing, resulting in a change of the effective refractive index of the silicon waveguides of ~0.01 which induces a 6.5 nanometer red shift of the AWG transmission spectrum, which matches our measurement results (5 nm-7 nm).
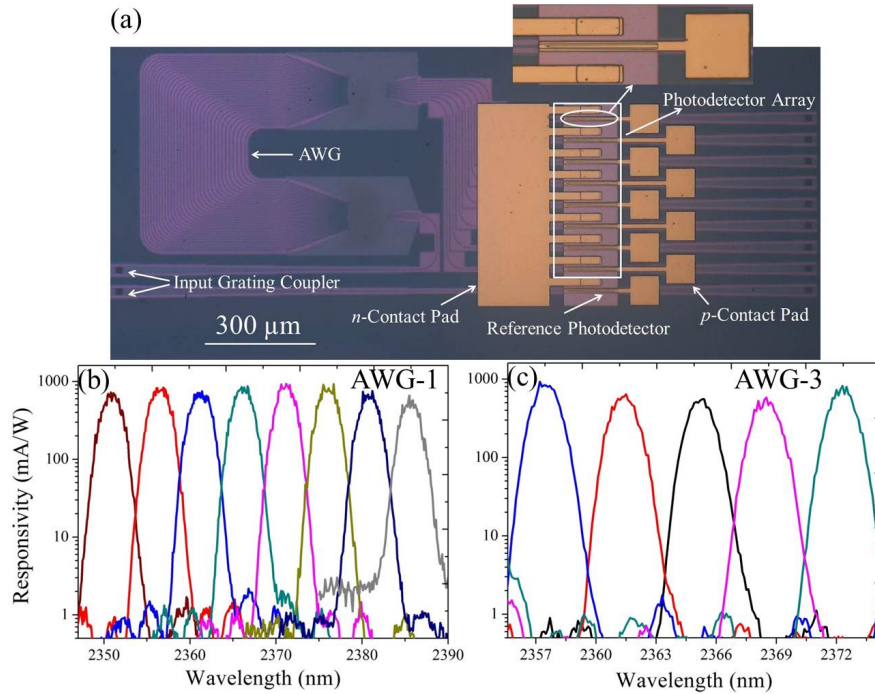
Fig. 7. (a) Microscope image of an AWG integrated with adiabatically-coupled photodetectors; (b) and (c) response of two AWG spectrometers with integrated photodetectors.

5. AWGs integrated with a grating-assisted photodetector array

Figure 8(a) shows the schematic of a grating-assisted InP-based type-II photodetector. In this design, light is coupled from a SOI waveguide into the III-V active region bonded on top by using a grating to diffract the light out of the SOI waveguide. The top p-contact layer (Ti/Au) has a high reflectivity at the device operating wavelength thereby enhancing the photoresponse. The size of the diffraction grating used in this work is 20 µm × 20 µm, and has a period of 1 µm and duty cycle of 50%. The size of the photodetector mesa is 25 µm × 25 µm. Compared with an adiabatically-coupled photodetector, this design has better III-V processing tolerance, as a very sharp taper tip is not required and a larger misalignment can be tolerated. A SEM image of the photodetector cross section is shown in Fig. 8(b). A 100 nm DVS-BCB layer is used for adhesive bonding.
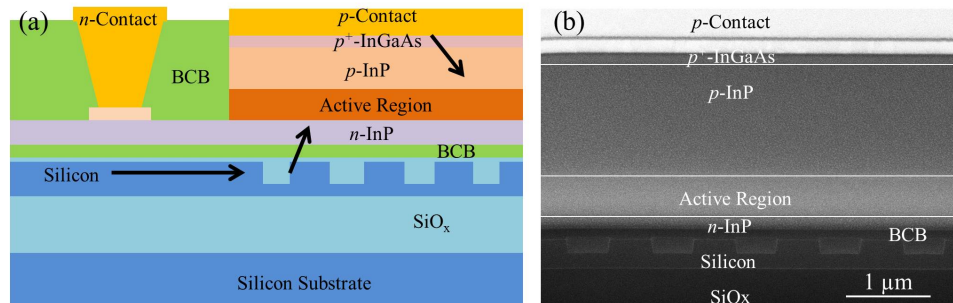

Fig. 8. (a) Schematic cross-section of the grating-assisted photodetector; (b) SEM image of the device cross-section.

A typical I-V characteristic of the grating-assisted photodetectors without light input at room temperature is shown in Fig. 9(a). The dark current is half of that in adiabatically-coupled photodetectors, around −5 nA at −0.5 V, which is attributed to the smaller perimeter of the grating-assisted devices compared to that of the adiabatically coupled devices. As the reverse voltage increase to 3 V, the dark current is still below 35 nA. Figure 9(b) shows the I-V characteristic of the photodetector under different waveguide-coupled input power levels at 2.35 μm wavelength. The heterogeneously integrated photodetectors behave linearly under 0 V bias as the input power increases until the maximum available output power of our light source (~630 μW). The waveguide-referred responsivity is around 0.1 A/W. This value is much lower than that of the adiabatically-coupled devices. For the adiabatically-coupled photodetector, light is efficiently coupled from the silicon waveguide to the active region (simulated to be above 90%) and fully absorbed along the III-V waveguide. In the grating-assisted photodetector, the responsivity is determined by up-coupling efficiency of grating coupler (simulated to be 40%) and the active region thickness. The active region in this epitaxial layer stack is a very thin multiple quantum wells stack(~100 nm), thereby leading to a low responsivity. The responsivity of the grating-assisted photodetector can be improved by increasing the thickness of the absorbing active region and introducing a mirror below the diffraction grating, to enhance the directionality of the grating coupler [18].
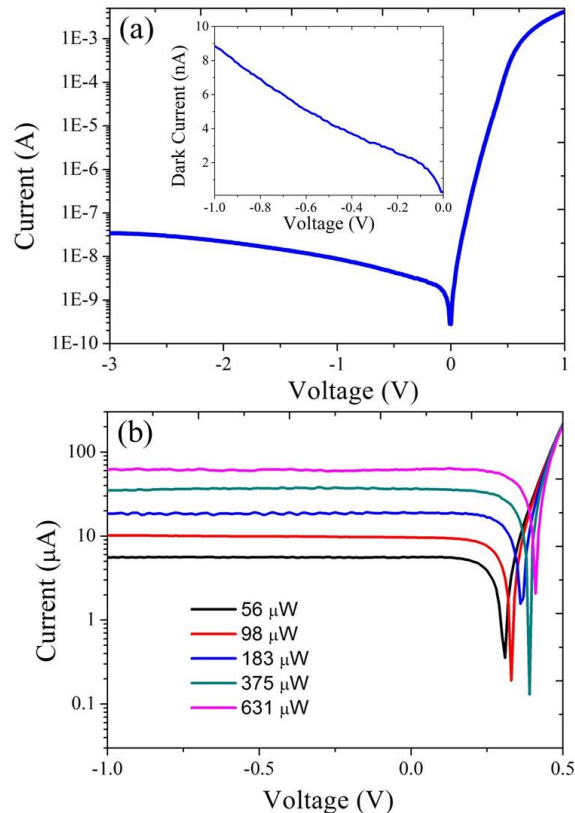

Fig. 9. (a) I-V characteristic of the photodetector in the dark, the inset picture shows the device dark current as a function of reverse bias; (b) I-V curve of the device under different waveguide-coupled input power levels.

Figure 10(a) shows a microscope picture of the 8-channel high resolution AWG (AWG-2, shown in Fig. 1(c)) integrated with grating-assisted photodetectors. All of the photodetectors share a common *n*-contact, and an individual *p*-contact. The pitch of the photodetectors is 60 μm, the same as the adiabatically-coupled devices. Figure 10(b) and 10(c) shows the

measured waveguide-referred responsivity as a function of wavelength for all of the channels in AWG-2 and AWG-4, respectively. Insertion loss can be obtained by normalizing the responsivity with the reference photodetector. The high resolution AWG-2 exhibits an insertion loss of 3 dB and crosstalk levels of −24 dB after III-V heterogeneous intergration processes. For the 12 channel AWG-4 device, an insertion loss of 3 dB and a crosstalk level of −23 dB is obtained.
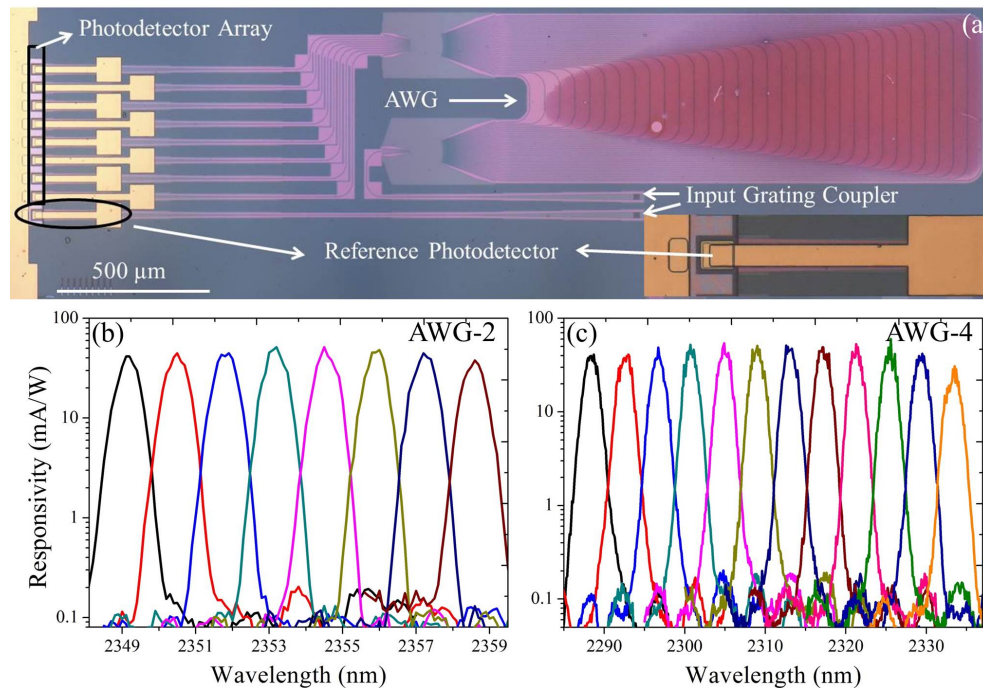

Fig. 10. (a) Microscope image of the high resolution AWG integrated with grating-assisted photodetectors; (b) and (c) measurement results of AWG-2 and AWG-4 integrated with grating-assisted photodetectors.

6. Conclusion

2-µm-wavelength-range wavelength demultiplexers based on SOI AWGs heterogeneously integrated with InP-based type-II quantum well photodetectors are reported. AWGs operating in the 2.3-2.4 µm wavelength range with different resolution and channel numbers are fabricated on a 400 nm thick SOI waveguide platform. Low insertion loss of 2.5-3 dB and low crosstalk of −30 to −25 dB are obtained for all of these passive AWGs. InP-based type-II photodetectors are heterogeneously integrated with the SOI AWGs, using two different coupling mechanisms. Adiabatically-coupled photodetectors have a high responsivity of 1.6 A/W at 2.35 µm wavelength and a dark current of 10 nA under a bias voltage of −0.5 V at room temperature. Grating-assisted photodetectors show a responsivity of 0.1 A/W and dark current of 5 nA. The performance of the wavelength demultiplexers does not degrade after photodetector array integration. A heterogeneously integrated light source is also realized by using the same epitaxial layer stack of the photodetectors. It enables the realization of a fully integrated 2-µm-wavelength-range spectroscopic system on silicon photonics.

Acknowledgments